

$\Sigma_c N$ interaction in chiral perturbation theory

Lu Meng,^{1,*} Bo Wang,^{2,1,†} and Shi-Lin Zhu^{1,2,‡}

¹*School of Physics and State Key Laboratory of Nuclear Physics and Technology, Peking University, Beijing 100871, China*

²*Center of High Energy Physics, Peking University, Beijing 100871, China*

We adopt the heavy baryon chiral perturbation theory to calculate the $\Sigma_c N$ interaction to the next-to-leading order. We consider the contact interactions, one-pion-exchange contributions, two-pion-exchange diagrams, and renormalization effects of the vertices, masses and wave functions. With the pion mass dependent expression, we fit the $\Sigma_c N$ interaction from HAL QCD calculation with $m_\pi \approx 410$ MeV and $m_\pi \approx 570$ MeV, and then extrapolate it to the physical pion mass. The ${}^3S_1(I = 1/2)$ $\Sigma_c N$ interaction is weakly attractive but no bound solution is found. We also propose a quark model to estimate the leading order $\Sigma_c N$ contact interaction with the NN interaction as input. This approach combining the quark model and the chiral effective field theory predicts a very attractive interaction in ${}^1S_0(I = 3/2)$ $\Sigma_c N$ channel and a two-body bound state.

I. INTRODUCTION

In the past decade, many novel hadronic states in the charm sector have been observed in experiments. Theoretical analysis revealed that some of these states might be the bound states or resonances of two heavy hadrons (for recent reviews, see Refs. [1–6]). Thus, the investigation on the hadron-hadron interaction is an important ingredient to understand these exotic structures.

Nuclear force is the best-understood hadron-hadron interaction, which has been extensively studied. More than eighty years ago, Yukawa proposed the one-pion-exchange interaction, which is the first clear picture about nuclear force [7]. The idea was then developed by including other meson-exchange interactions or operators to obtain the nuclear force with high precision [8–10]. The modern theory to build the nuclear force is the chiral perturbation theory (ChPT) [11, 12], which is another inheritor of Yukawa’s idea. The formalism originates from Weinberg [13, 14], in which the nuclear force can be calculated order by order. The two-pion-exchange loop diagrams even multi-pion-exchange ones could be considered by the arrangement of power counting. Apart from these frameworks at the hadron level, the quark model was also exploited to calculate the nuclear force [15–26]. Quark model could provide some insights into the origin of the repulsive core of nuclear force [16–18, 23]. Recently, the HAL QCD collaboration proposed a framework to calculate the nuclear force from the lattice QCD simulations [27–29]. The methods mentioned above in calculating the nuclear force were also extended to study other hadron-hadron interactions [30–46].

Investigating the $Y_c N$ ($Y_c = \Sigma_c$ or Λ_c) interaction is a natural extension of the NN interaction, which is important to explore the properties of charmed baryons in nuclear matter [47]. Meanwhile, there is a long history to study the charmed hypernuclei [48–50]. The conventional nuclei would become the charmed one when one or more inner nucleons are replaced by the charmed baryons. The charmed hypernuclei is an analogy of strange hypernuclei. The $Y_c N$ interaction is a

cornerstone to understand the charmed hypernuclei. Recently, the experimental proposals at J-PARC [51, 52] and FAIR [53] on the charmed hypernuclei also inspired numerous theoretical researches on the $Y_c N$ interactions and charmed hypernuclei [54–66]. See Refs. [47, 67] for recent reviews.

In Ref. [59], the OBE model was adopted to calculate the $Y_c N$ potential. The molecular bound states of $\Lambda_c N$ were obtained with the essential couple-channel effect from $\Sigma_c N$ and $\Sigma_c^* N$. In Ref. [62], the $Y_c N$ and $Y_b N$ potentials were calculated within the framework of the quark delocalization color screening model (QDCSM). The results showed that the attraction between N and $\Lambda_{c/b}$ is too weak to form the bound states even with the couple-channel effect. The $\Sigma_{c/b} N({}^3S_1)$ resonance was obtained by coupling to the D -wave $\Lambda_c N$ channel. In Ref. [63], a constituent quark model was performed to study the $Y_c N$ interaction, which points to the soft interaction without two-body bound states and weak couple-channel effect. In Refs. [60, 61], a potential model ($Y_c N$ CTNN) combining the OBE model and quark model was constructed. The model contains a long-range meson exchange part (π and σ) and a short distance quark exchange part. It is interesting that the quark model [62, 63] and the OBE model [59] present different pictures about $Y_c N$ interaction.

In Refs. [64, 65], the HAL QCD collaboration presented the $\Lambda_c N$ potential and preliminary $\Sigma_c N$ potential from the lattice QCD simulations. These simulations from the first principle were performed in the quark mass corresponding to the pion masses $m_\pi = 410 - 700$ MeV. The $\Lambda_c N$ interaction from lattice QCD was extrapolated to the physical pion mass with the chiral effective field theory [66]. Rather than following the standard Weinberg’s power counting law, the authors omitted the two-pion exchange contribution at the next-to-leading order and included some high order contact terms. More refined calculation on $Y_c N$ interaction with less model-dependent framework is needed.

In this work, we adopt the heavy baryon chiral perturbation theory (HBChPT) to calculate the $\Sigma_c N$ interaction to the next-to-leading order. We consider the leading order contact interaction, one-pion-exchange contribution and the next-to-leading order contact interaction and two-pion-exchange diagrams. We include the $\Sigma_c^{(*)}$ as intermediate states in the loop diagrams. With the analytical results, we extrapolate the phase shift from HAL QCD to the physical pion mass and obtain the

* lmeng@pku.edu.cn

† bo-wang@pku.edu.cn

‡ zhushl@pku.edu.cn

$\Sigma_c N$ interaction with quantum number ${}^3S_1 (I = 1/2)$. We also use a quark model to relate the leading-order contact interaction of $\Sigma_c N$ to those of NN systems. In this approach, combining the quark model and HBChPT, we give the numerical results of the S -wave $\Sigma_c N$ interaction.

This paper is arranged as follows. In Sec. II, we construct the Lagrangians. In Sec. III, we calculate the analytical results of the $\Sigma_c N$ interaction to the next-to-leading order. We discuss the pion mass dependence of our analytical results in Sec. IV, and extrapolate the lattice QCD results to the physical pion mass in Sec. V. We give a brief conclusion in Sec. VI. In Appendix A, we combine the quark model and analytical results from HBChPT to give more predictions on the $\Sigma_c N$ interaction. In Appendix B, we present the integrals used in our calculation.

II. EFFECTIVE LAGRANGIANS AND WEINBERG'S FORMALISM

We perform the chiral expansion in the framework of HBChPT. The expansion is organized in powers of $\epsilon = q/\Lambda_\chi$, where q is either the momenta of Goldstone bosons or the residual momenta of the matter fields. Λ_χ is the chiral symmetry breaking scale. We calculate the scattering amplitude order by order according to the power counting given by Weinberg [13, 14]. In our calculation, we include the Σ_c^* , the heavy quark spin symmetry partner of Σ_c as the intermediate states. In the analytical calculations, we keep the mass splitting $\delta_1 = M_{\Sigma_c^*} - M_{\Sigma_c}$.

The amplitudes of box diagrams would blow up in the heavy baryon limit, which would also be amplified to destroy the power counting even if we include the kinetic terms of the heavy baryon. Thus, we adopt the Weinberg's formalism to deal with this problem [13, 14, 40, 41, 68]. We subtract the two particle reducible (2PR) contribution in the box diagrams, which could be generated by iterating the one-pion-exchange diagrams. The remaining two particle irreducible (2PIR) part obeys the power counting, which is treated as the kernel of the Lippmann-Schwinger equation or Schrödinger equation.

We introduce the pion field and the involved building blocks as follows,

$$\phi = \sqrt{2} \begin{pmatrix} \frac{\pi^0}{\sqrt{2}} & \pi^+ \\ \pi^- & -\frac{\pi^0}{\sqrt{2}} \end{pmatrix}, U = u^2 = \exp\left(i \frac{\phi(x)}{F}\right), \quad (1)$$

$$\Gamma_\mu = \frac{1}{2} [u^\dagger, \partial_\mu u], \quad u_\mu = \frac{i}{2} \{u^\dagger, \partial_\mu u\}, \quad (2)$$

where the Γ_μ and u_μ are the chiral connection and axial-vector current, respectively. F is the pion decay constant.

The multiplets of spin- $\frac{1}{2}$ Σ_c and spin- $\frac{3}{2}$ Σ_c^* are represented as

$$\Sigma_c = \begin{pmatrix} \Sigma_c^{++} & \frac{\Sigma_c^+}{\sqrt{2}} \\ \frac{\Sigma_c^+}{\sqrt{2}} & \Sigma_c^0 \end{pmatrix}, \quad \Sigma_c^{*\mu} = \begin{pmatrix} \Sigma_c^{*++} & \frac{\Sigma_c^{*+}}{\sqrt{2}} \\ \frac{\Sigma_c^{*+}}{\sqrt{2}} & \Sigma_c^{*0} \end{pmatrix}^\mu \quad (3)$$

The leading order Lagrangians associated with $\Sigma_c^{(*)}$ are constructed as

$$\begin{aligned} \mathcal{L}_{\Sigma_c^{(*)}\phi}^{(0)} = & \text{Tr}[\bar{\Sigma}_c(i\not{D} - M_{\Sigma_c})\Sigma_c] + \text{Tr}[\bar{\Sigma}_c^{*\mu}[-g_{\mu\nu}(i\not{D} - M_{\Sigma_c^*}) \\ & + i(\gamma_\mu D_\nu + \gamma_\nu D_\mu) - \gamma_\mu(i\not{D} + M_{\Sigma_c^*})\gamma_\nu]\Sigma_c^{*\nu}] \\ & + g_1 \text{Tr}[\bar{\Sigma}_c \gamma^\mu \gamma_5 u_\mu \Sigma_c] + g_3 \text{Tr}[\bar{\Sigma}_c^{*\mu} u_\mu \Sigma_c + \text{H.c.}] \\ & + g_5 \text{Tr}[\bar{\Sigma}_c^{*\nu} \gamma^\mu \gamma_5 u_\mu \Sigma_c^*], \end{aligned} \quad (4)$$

where $\text{Tr}[\dots]$ represents the trace in the flavor space. M_{Σ_c} and $M_{\Sigma_c^*}$ denote the masses of Σ_c and Σ_c^* , respectively. The covariant derivative is defined as $D_\mu \Sigma_c^{(*)} = \partial_\mu \Sigma_c^{(*)} + \Gamma_\mu \Sigma_c^{(*)} + \Sigma_c \Gamma_\mu^{(*)T}$. The g_1 , g_3 and g_5 are axial coupling constants. We can define the superfield to set up the relation of Σ_c and Σ_c^* in the heavy quark limit,

$$\begin{aligned} \psi^\mu &= \mathcal{B}^{*\mu} - \sqrt{\frac{1}{3}}(\gamma^\mu + v^\mu)\gamma^5 \mathcal{B}, \\ \bar{\psi}^\mu &= \bar{\mathcal{B}}^{*\mu} + \sqrt{\frac{1}{3}}\bar{\mathcal{B}}\gamma^5(\gamma^\mu + v^\mu), \end{aligned} \quad (5)$$

where $\mathcal{B}^{(*)}$ are the $\Sigma_c^{(*)}$ fields after heavy baryon reduction. The Lagrangians can be rewritten as a more compact form with the superfield,

$$\begin{aligned} \mathcal{L}_{\Sigma_c\phi}^{(0)} = & -\text{Tr}[\bar{\psi}^\mu i v \cdot D \psi_\mu] + i g_a \epsilon_{\mu\nu\rho\sigma} \text{Tr}[\bar{\psi}^\mu u^\rho v^\sigma \psi^\nu] \\ & + i \frac{\delta_1}{2} \text{Tr}[\bar{\psi}^\mu \sigma_{\mu\nu} \psi^\nu]. \end{aligned} \quad (6)$$

where the third term represents the heavy quark spin symmetry violation effect. $\delta_1 = M_{\Sigma_c^*} - M_{\Sigma_c}$ is the mass splitting between Σ_c and Σ_c^* . Comparing Eq. (6) with Eq. (4), one can easily get

$$g_1 = -\frac{2}{3}g_a, \quad g_3 = -\sqrt{\frac{1}{3}}g_a, \quad g_5 = g_a. \quad (7)$$

The leading order Lagrangians for nucleons can be constructed as

$$\mathcal{L}_{N\phi}^{(0)} = \bar{N}(i\not{D} - M_N)N + g_A \bar{N} \gamma^\mu \gamma_5 u_\mu N, \quad (8)$$

where $N = (p, n)^T$ is the nucleon isospin doublet. M_N and g_A are the nucleon mass and axial coupling constant, respectively. The covariant derivative is define as $\mathcal{D}_\mu = \partial_\mu + \Gamma_\mu$.

At the leading order, the contact terms also contribute to the $\Sigma_c N$ interaction. The independent Lagrangians read

$$\begin{aligned} \mathcal{L}_{\text{contact}}^{(0)} = & C_3 \bar{N} N \text{Tr}(\bar{\psi}^\mu \psi_\mu) + C_4 (\bar{N} \boldsymbol{\tau} N) \cdot \text{Tr}(\bar{\psi}^\mu \boldsymbol{\tau} \psi_\mu) \\ & + i \frac{3}{2} \tilde{C}_3 (\bar{N} \sigma_{\mu\nu} N) \text{Tr}(\bar{\psi}^\mu \psi^\nu) \\ & + i \frac{3}{2} \tilde{C}_4 (\bar{N} \boldsymbol{\tau} \sigma_{\mu\nu} N) \cdot \text{Tr}(\bar{\psi}^\mu \boldsymbol{\tau} \psi^\nu), \end{aligned} \quad (9)$$

where $\boldsymbol{\tau}$ is the Pauli matrix in the isospin space. C_3 , \tilde{C}_3 , C_4 and \tilde{C}_4 are the low energy constants (LECs).

III. EFFECTIVE POTENTIALS

We calculate the $\Sigma_c N$ effective potential $\mathcal{V}(\mathbf{q})$ in the momentum space to the next-to-leading order. The chiral dynamics is essentially the interplay of the light degrees of freedom. For the $\Sigma_c^{(*)} N$ system, the elements of the interaction are the spin triplet light diquark in $\Sigma_c^{(*)}$ and N . In the calculation, we include both Σ_c and Σ_c^* as the intermediate states to ensure the whole spin triplet light diquark is considered. The Λ_c and $\Sigma_c^{(*)}$ belong to the different isospin multiplets. The Λ_c plays the similar role as the Δ in the NN system [69]. In this work, we include neither the Δ nor the Λ_c as intermediate states.

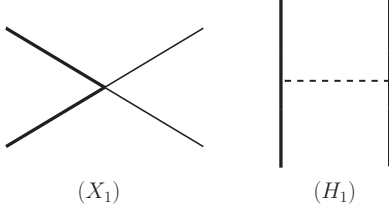


FIG. 1. The leading order diagrams for the $\Sigma_c N$ system. At this order, the contact term (X_1) and the one-pion-exchange diagram (H_1) contribute to the effective potential. The solid, thick solid and dashed lines represent the N , Σ_c and pion, respectively.

The leading order $\mathcal{O}(\epsilon^0)$ potential of $\Sigma_c N$ arises from the tree level contact and one-pion-exchange diagrams in Fig. 1. The leading order potential reads

$$\mathcal{V}_{X_1}^{(0)} = C_3 + 2C_4 \mathbf{I}_1 \cdot \mathbf{I}_2 + (\tilde{C}_3 + 2\tilde{C}_4 \mathbf{I}_1 \cdot \mathbf{I}_2) \boldsymbol{\sigma}_1 \cdot \boldsymbol{\sigma}_2,$$

$$\mathcal{V}_{H_1}^{(0)} = -\frac{g_A g_1}{2F^2} (\mathbf{I}_1 \cdot \mathbf{I}_2) \frac{(\boldsymbol{\sigma}_1 \cdot \mathbf{q})(\boldsymbol{\sigma}_2 \cdot \mathbf{q})}{\mathbf{q}^2 + m^2}, \quad (10)$$

where the subscript X_1 and H_1 denote the label of Feynman diagrams. The m is the pion mass. $\mathbf{I}_1 \cdot \mathbf{I}_2$ and $\boldsymbol{\sigma}_1 \cdot \boldsymbol{\sigma}_2$ are the isospin-isospin and spin-spin operators, respectively. Their matrix elements are calculated as

$$\begin{aligned} \langle \mathbf{I}_1 \cdot \mathbf{I}_2 \rangle &= \frac{1}{2} [I(I+1) - I_1(I_1+1) - I_2(I_2+1)], \\ \langle \boldsymbol{\sigma}_1 \cdot \boldsymbol{\sigma}_2 \rangle &= 2[S(S+1) - S_1(S_1+1) - S_2(S_2+1)]. \end{aligned}$$

Since we only focus on the S -wave $\Sigma_c N$ system, we can take the following replacement,

$$q^i q^j \mapsto \frac{1}{3} \mathbf{q}^2 \delta^{ij}. \quad (11)$$

The next-to-leading order potential arises from the $\mathcal{O}(\epsilon^2)$ tree level contact term, the two-pion-exchange interaction and the renormalization of the $\mathcal{O}(\epsilon^0)$ diagrams. One can construct the general contact interaction [70]. In this work, we only concentrate on the S -wave interaction and omit the recoil terms. Thus, the next-to-leading order contact potential reads

$$\begin{aligned} \mathcal{V}_{X_1}^{(2)} &= (C_5 + C_6 \mathbf{I}_1 \cdot \mathbf{I}_2) \mathbf{q}^2 \\ &\quad + (\tilde{C}_5 + \tilde{C}_6 \mathbf{I}_1 \cdot \mathbf{I}_2) \mathbf{q}^2 (\boldsymbol{\sigma}_1 \cdot \boldsymbol{\sigma}_2), \end{aligned} \quad (12)$$

where C_5 , C_6 , \tilde{C}_5 and \tilde{C}_6 are LECs in the $\mathcal{O}(\epsilon^2)$ contact Lagrangians.

At the next-to-leading order, the two-pion-exchange contributions read

$$\mathcal{V}_{F_1}^{(2)} = \frac{1}{F^4} (\mathbf{I}_1 \cdot \mathbf{I}_2) J_{22}^F, \quad (13)$$

$$\mathcal{V}_{T_1}^{(2)} = \frac{-4g_A^2}{F_0^4} (\mathbf{I}_1 \cdot \mathbf{I}_2) \left[\frac{1}{4} \mathbf{q}^2 (J_{24}^T + J_{33}^T) + \frac{1-d}{4} J_{34}^T \right] (0), \quad (14)$$

$$\mathcal{V}_{T_2}^{(2)} = \frac{-g_1^2}{F_0^4} (\mathbf{I}_1 \cdot \mathbf{I}_2) \left[\frac{1}{4} \mathbf{q}^2 (J_{24}^T + J_{33}^T) + \frac{1-d}{4} J_{34}^T \right] (0), \quad (15)$$

$$\mathcal{V}_{T_3}^{(2)} = \frac{g_3^2}{4F^4} (\mathbf{I}_1 \cdot \mathbf{I}_2) \left[J_{34}^T (d-2) + (J_{33}^T + J_{24}^T) \mathbf{q}^2 \frac{2-d}{d-1} \right] (-\delta_1), \quad (16)$$

$$\begin{aligned} \mathcal{V}_{B_1}^{(2)} &= \frac{g_A^2 g_1^2}{F^4} 2(1 - \mathbf{I}_1 \cdot \mathbf{I}_2) \left\{ J_{41}^B \left[\left(\frac{1-d}{4} \right)^2 + \frac{3}{8} \right] - (J_{42}^B + J_{31}^B) \frac{1+d}{8} \mathbf{q}^2 - J_{21}^B \frac{1}{16} \mathbf{q}^2 \right. \\ &\quad \left. + (J_{43}^B + 2J_{32}^B + J_{22}^B) \frac{1}{16} \mathbf{q}^4 + [(\boldsymbol{\sigma}_1 \cdot \boldsymbol{\sigma}_2) \mathbf{q}^2 - \mathbb{T}] J_{21}^B \mathbf{q}^2 \right\} (0, 0), \end{aligned} \quad (17)$$

$$\begin{aligned} \mathcal{V}_{B_2}^{(2)} &= -\frac{g_A^2 g_3^2}{8F^4} (1 - \mathbf{I}_1 \cdot \mathbf{I}_2) \left\{ J_{41}^B \left[(1-d)d + \frac{6}{(d-1)} \right] + (J_{42}^B + J_{31}^B) \frac{2(d-2)(d+1)}{(d-1)} \mathbf{q}^2 + J_{21}^B \frac{d-2}{d-1} \mathbf{q}^2 \right. \\ &\quad \left. + (J_{43}^B + 2J_{32}^B + J_{22}^B) \frac{2-d}{d-1} \mathbf{q}^4 + [(\boldsymbol{\sigma}_1 \cdot \boldsymbol{\sigma}_2) \mathbf{q}^2 - \mathbb{T}] J_{21}^B \frac{\mathbf{q}^2}{d-1} \right\} (-\delta_1, 0), \end{aligned} \quad (18)$$

$$\mathcal{V}_{R_i}^{(2)} = \mathcal{V}_{B_i}^{(2)} \Big|_{J_x^B \rightarrow J_x^R, \mathbf{I}_1 \cdot \mathbf{I}_2 \rightarrow -\mathbf{I}_1 \cdot \mathbf{I}_2, \boldsymbol{\sigma}_1 \cdot \boldsymbol{\sigma}_2 \rightarrow -\boldsymbol{\sigma}_1 \cdot \boldsymbol{\sigma}_2}, \quad (19)$$

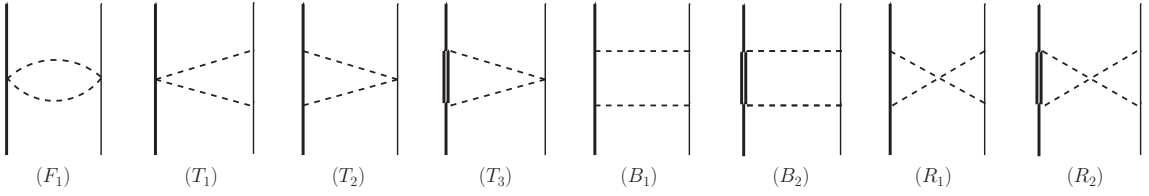


FIG. 2. The two-pion-exchange diagrams for the $\Sigma_c N$ system. There is one football diagram (F_1), three triangle diagrams ($T_{1,2,3}$), two box diagrams ($B_{1,2}$) and two crossed box diagrams ($R_{1,2}$). The solid, thick solid, double thick solid and dashed lines represent the N , Σ_c , Σ_c^* and pion fields, respectively.

where d is the dimension in the dimensional regularization. $\mathbb{T} = (\boldsymbol{\sigma}_1 \cdot \mathbf{q})(\boldsymbol{\sigma}_2 \cdot \mathbf{q})$. J_{ij}^X are the loop integrals defined in the Appendix B. They are the functions of m , \mathbf{q}^2 and mass splitting. For conciseness, we omit the m and \mathbf{q}^2 and keep the specific mass splitting at the end of every expression.

The vertex renormalization, mass renormalization and wave function renormalization of the leading order diagrams will also contribute to the next-to-leading order potential. The renormalizations of the one-pion-exchange diagram and the leading order contact term are presented in Figs. 4 and 5, respectively. When we calculate the $\Sigma_c N$ potential at the physical pion mass, these renormalization effects can be included by adopting the physical hadron masses and coupling constants in the tree level results. When we vary the pion mass, these renormalization effects will induce the extra pion mass dependence. We will discuss these renormalization diagrams in the next section.

IV. PION MASS DEPENDENCE

The $\Sigma_c N$ potentials depend on the pion mass either explicitly in expressions of Sec. III, or implicitly through the decay constants, the LECs, the mass of baryons and the renormalization of wave functions.

The m_π -dependence for the pion decay constant can be obtained in the framework of ChPT. It was shown that the next-to-leading SU(2) results can not fit the m_π -dependent decay constant from lattice QCD well in FIG. 3 of Ref. [71]. As shown in FIG. 5 of Ref. [71], one needs to calculate at least to the next-to-next-to-leading order to depict the m_π -dependence, which is beyond the precision of this work. Rather than going to higher order calculation, we fit the lattice results with a linear function of m_π^2 . The result is shown in Fig. 3. The simple linear function can depict the m_π -dependence rather well at least when the pion mass is less than 500 MeV.

The renormalization of one-pion-exchange diagram would contribute to the next-to-leading order amplitude,

$$\mathcal{A}_{\text{ope}}^r = (1 + \delta Z_\pi + \delta Z_N + \delta Z_{\Sigma_c}) \mathcal{A}_{\text{ope}}(g_i^r, m_r), \quad (20)$$

where g_i^r and the m_r denote the renormalized axial coupling constants and hadron masses. The δZ_π , δZ_N and δZ_{Σ_c} arise from the wave function renormalization of π , N and Σ_c , respectively.

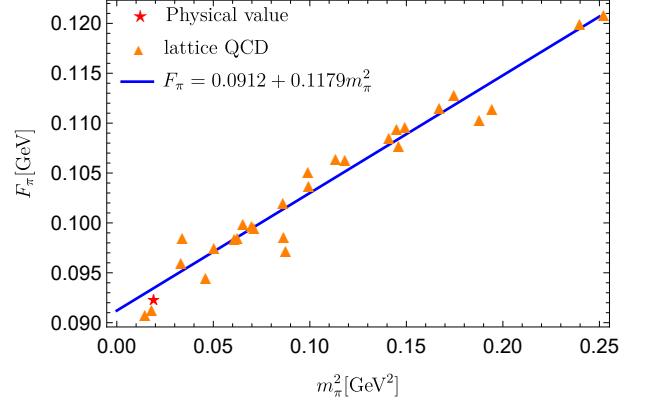


FIG. 3. The m_π -dependence of pion decay constant from Ref. [71] and a linear fit in this work. For the lattice QCD results, we only give the central value here.

Up to the next-to-leading order, the m_π -dependence of renormalized g_1^r and g_A^r can also be obtained by calculating the vertex renormalization diagrams (e_1)–(e_7) in Fig. 4. The results read

$$g_A^r = g_A(1 + \delta Z_{g_A}), \quad g_1^r = g_1(1 + \delta Z_{g_1}), \quad (21)$$

$$\delta Z_{g_A} = -\frac{J_0^c}{3F^2} - \frac{d-3}{4} \frac{g_A^2}{F^2} J_{22}^g(0,0), \quad (22)$$

$$\begin{aligned} \delta Z_{g_1} = & -\frac{J_0^c}{3F^2} + \frac{d-3}{4} \frac{g_1^2}{F^2} J_{22}^g(0,0), \\ & + \left[(d-3) + \left(\frac{d-3}{d-1} \right)^2 \right] \frac{g_3^2 g_5}{4F^2 g_1} J_{22}^g(-\delta_1, -\delta_1) \\ & + \frac{g_3^2}{F^2} \frac{2-d}{d-1} J_{22}^g(-\delta_1, 0). \end{aligned} \quad (23)$$

The lattice QCD simulation in Refs. [72–74] showed that the g_A^r and g_1^r are insensitive to the pion mass. Thus, we keep the axial coupling constants g_1 and g_A invariant with the change of the pion mass.

The field renormalization diagrams (d_1), (e_1), (e_2) and (e_3) in Fig. 4 would give the wave function renormalization and mass renormalization. The mass renormalization effects are included by adopting the m_π -dependent hadron masses in Table I. The wave function renormalizations read

$$\delta Z_\pi = \frac{2J_0^c}{3F^2}, \quad (24)$$

TABLE I. Hadron masses at different pion mass (in units of MeV) [65].

m_π	m_N	m_{Σ_c}	$m_{\Sigma_c^*}$	δ_1
139	938	2454	2518	64
412	1215	2575	2661	86
570	1399	2674	2763	89
702	1581	2780	2866	86

$$\delta Z_N = \frac{g_A^2}{F^2} \frac{3(1-d)}{4} \frac{\partial J_{22}^a(\omega)}{\partial \omega} \Big|_{\omega=0}, \quad (25)$$

$$\begin{aligned} \delta Z_{\Sigma_c} &= \frac{g_1^2}{F^2} \frac{1-d}{2} \frac{\partial J_{22}^a(\omega)}{\partial \omega} \Big|_{\omega=0} \\ &+ \frac{g_3^2}{F^2} \frac{2-d}{2} J_{22}^a \frac{\partial J_{22}^a(\omega)}{\partial \omega} \Big|_{\omega=-\delta_1}. \end{aligned} \quad (26)$$

Eqs. (24)-(26) would bring extra m_π -dependence to the potential.

In Fig. 5, we present the Feynman diagrams contributing to the renormalization of contact terms. The (g_i) and (h_i) diagrams would renormalize the leading order contact terms,

$$C_i^r = C_i + \delta C_i. \quad (27)$$

In the heavy quark limit and with $d \rightarrow 4$, δC_i read

$$\begin{aligned} \delta C_3 &= \frac{1}{F^2} J_{22}^g \left[-C_3 g_a^2 - C_3 \frac{9}{4} g_A^2 \right], \\ \delta \tilde{C}_3 &= \frac{1}{F^2} J_{22}^g \left[-\frac{13}{36} \tilde{C}_3 g_a^2 + \frac{3}{4} \tilde{C}_3 g_A^2 + (\tilde{C}_3 + 2\tilde{C}_4) g_a g_A \right], \\ \delta C_4 &= \frac{1}{F^2} J_{22}^g \left[-\frac{1}{2} C_4 g_a^2 - \frac{9}{8} C_4 g_A^2 + 3\tilde{C}_4 g_a g_A \right], \\ \delta \tilde{C}_4 &= \frac{1}{F^2} J_{22}^g \left[-\frac{13}{72} \tilde{C}_4 g_a^2 + \frac{3}{8} \tilde{C}_4 g_A^2 + \frac{2}{3} C_4 g_a g_A \right], \end{aligned} \quad (28)$$

where the J_{22}^g has the finite terms,

$$J_{22}^g = -\frac{1}{16\pi^2(d-1)} \left[2m^2 + 3m^2 \ln \frac{m^2}{\lambda^2} \right]. \quad (29)$$

where λ is the chiral symmetry breaking scale Λ_χ . When the spin and the isospin of $\Sigma_c N$ are fixed, the m_π -dependent contact interaction can be reparameterized as

$$\begin{aligned} \mathcal{V}_{\text{contact}} &= c_1 (1 + \delta Z_N + \delta Z_{\Sigma_c}) \\ &+ \tilde{c}_1 \frac{m^2}{F^2} \left(2 + 3 \ln \frac{m^2}{\lambda^2} \right) + c_2 \mathbf{q}^2 + c_3 m^2, \end{aligned} \quad (30)$$

where the c_1 terms denote the leading order interaction and its wave function renormalization. The \tilde{c}_1 terms represent the renormalization of the leading order contact coupling constants. The c_2 and c_3 terms arise from the next-to-leading order tree diagrams.

V. NUMERICAL RESULTS

We keep the mass splitting between Σ_c^* and Σ_c when we calculate the analytical results. In the real physical world, the mass splitting $\delta_1 \simeq 64$ MeV is of the same order as the physical pion mass. Thus, we can adopt the small-scale-expansion and treat the δ_1 as another small scale like the pion mass [75]. However, when we go to the world with much heavier pion as shown in Table I, the mass splitting become much less than the pion mass. The small-scale-expansion for δ_1 does not work any more. Thus, in this work, we take the heavy quark limit and omit the mass splitting δ_1 . The 2PR contribution in the box diagram (B_2) of Fig. 2 and diagram (h_2) of Fig. 5 should be subtracted, which is different from our previous works [40, 41].

In this work, we choose the m_π -dependent chiral symmetry breaking scale $\Lambda_\chi = 4\pi F(m_\pi)$. An alternative approach to the m_π -dependent Λ_χ is the mass of ρ meson [76, 77], which brings the slight divergence from the former one. To ensure the good chiral convergence, we only adopt the lattice QCD results with $m_\pi \approx 410$ MeV and 570 MeV in Ref. [65].

With the potential in the momentum space, the potential in the coordinate space reads

$$V(r) = \frac{1}{(2\pi)^3} \int d^3 \mathbf{q} e^{i\mathbf{q}\cdot\mathbf{r}} \mathcal{V}(\mathbf{q}) \mathcal{F}(\mathbf{q}). \quad (31)$$

where $\mathcal{F}(\mathbf{q}) = \exp(-\mathbf{q}^{2n}/\Lambda^{2n})$ is the regulator to suppress the contribution of the high momentum [12, 42, 78]. In this work, we choose two different regulators. In scenario I, we adopt $n = 1$ and $\Lambda = 0.8$ GeV. In scenario II, we adopt $n = 2$ and $\Lambda = 0.5$ GeV.

We then calculate the phase shift from the potential, which is the physical observable. The partial wave Lippmann-Schwinger equation reads [79]

$$\begin{aligned} \psi_l^P(k, r) &= u_l(kr) + 2\mu \int_0^\infty dr' G_l^P(k; r, r') V(r') \psi_l^P(k, r'), \\ G_l^P &= k^{-1} u_l(kr_<) v_l(kr_>), \end{aligned} \quad (32)$$

where $u_l(kr)$ and $v_l(kr)$ are Riccati-Bessel function and Riccati-Neumann function, respectively. $r_> = \max\{r, r'\}$ and $r_< = \min\{r, r'\}$. The superscript “P” denotes the Green function and the wave functions are the principal-value ones. The K -matrices and the phase shifts can be obtained by

$$K_l = \tan \delta_l = -2\mu k^{-1} \int_0^\infty dr u_l(kr) V(r) \psi_l^P(k, r). \quad (33)$$

The scattering length could be obtained by performing the effective-range expansion. For the S -wave, the expansion reads

$$k \cot \delta = -\frac{1}{a_s} + \frac{1}{2} k^2 r_e + \dots, \quad (34)$$

where a_s and r_e are the scattering length and the effective range, respectively.

The numerical results of phase shift are presented in Figs. 6 and 7 for scenario I and scenario II, respectively. We fit the

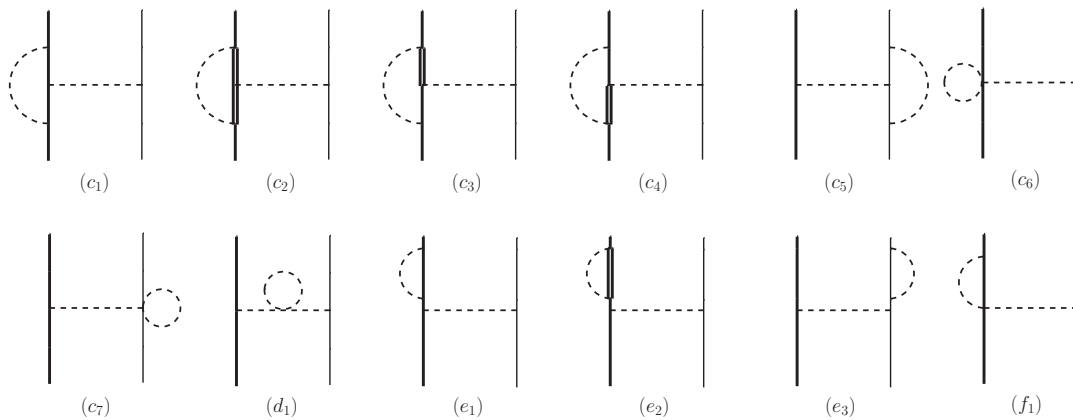


FIG. 4. The renormalization diagrams for the one-pion-exchange interaction. The (c_1) - (c_7) diagrams renormalize the axial coupling vertices. The (d_1) diagram renormalize the pion field. The (e_1) and (e_2) renormalize the Σ_c field. The (e_3) renormalize the N field. The (f_1) diagram vanishes. Notations are the same as those in Fig. 2.

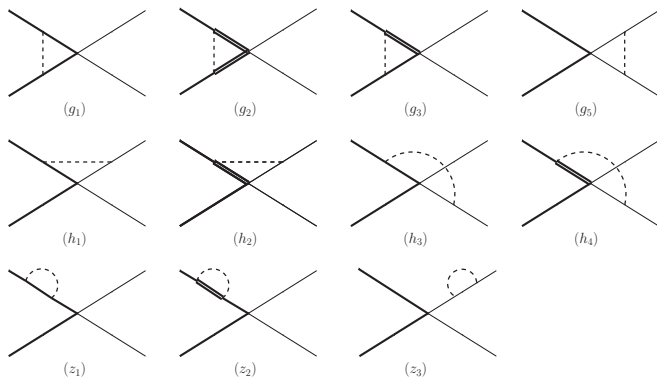


FIG. 5. The renormalization diagrams for contact interaction. The (g_i) and (h_i) diagrams are the contact vertices renormalization. The (z_i) diagrams are the wave function renormalization. Notations are the same as those in Fig. 2.

phase shift from lattice QCD results [65] with $m_\pi \approx 410$ MeV and $m_\pi \approx 570$ MeV to obtain the unknown LECs c_1 , \tilde{c}_1 , c_2 and c_3 [see Eq. (30)]. Only the $\Sigma_c N$ interaction with quantum number ${}^3S_1(I = 1/2)$ is available in lattice QCD [65]. Then, we obtain the phase shift of this channel at the physical pion mass. We show the potential in coordinate space in Fig. 8.

In two scenarios, we can fit the phase shifts well with our analytical results (see the first two graphs in Figs. 6 and 7). Thus, we grasp the main features of the m_π -dependent charmed baryon-nucleon interaction. We get similar chiral extrapolation results in two scenarios with different regulators. Potentials in two scenarios are both repulsive in the short range and attractive in the medium range, which is the same as the nuclear force. We also calculate the scattering lengths in two scenarios,

$$\begin{aligned} a_s &= -0.53_{-0.11}^{+0.10} \text{ fm (scenario I),} \\ a_s &= -1.83_{-0.42}^{+0.32} \text{ fm (scenario II).} \end{aligned} \quad (35)$$

The negative scattering length indicates the attractive $\Sigma_c N$ in-

teraction in ${}^3S_1(I = 1/2)$ channel. However, the attraction is very weak, i.e., there do not exist the bound solutions in both scenarios.

The different regulators in two scenarios do bring some differences to our results. In Fig. 8, the short-range repulsion in scenario I is much stronger than that in scenario II, while the medium-range attraction in scenario II is much stronger. Thus, both scattering lengths in two scenarios are negative but the one in scenario II has the larger absolute value. The differences stemming from the choice of the regulator do not change the results qualitatively.

In order to give the numerical results of other channels, we propose a quark model to estimate the leading order contact interaction with the NN interaction as inputs. In HBChPT, the two-pion-exchange diagrams mimic some heavy-meson-exchange contribution like ρ and σ in one-boson-exchange scheme. Thus, there are some ambiguities to use specific heavy meson exchanges to calculate the contact interaction. Meanwhile, the contact interaction obtained by contracting the specific heavy meson exchange diagram to one single vertex might not reproduce the NN phase shift well. To avoid the ambiguity and reduce the uncertainty, we do not consider the specific exchanged mesons but introduce the contact interaction at the quark level. The SU(3) flavor symmetry is used to reduce the number of coupling constants. The unknown coupling constants are determined by the NN interaction. In this way, we could make use of flavor symmetry to build a bridge between the $\Sigma_c N$ and NN interactions. The $\Sigma_c N$ potentials are shown in Fig. 9. The details about the quark model are given in Appendix A.

VI. CONCLUSION

In summary, we adopt the heavy baryon chiral perturbation theory to calculate the S -wave $\Sigma_c N$ interaction to the next-to-leading order. We consider the leading order contact term and one-pion-exchange interaction, the next-to-leading order contact term and two-pion-exchange contribution. At

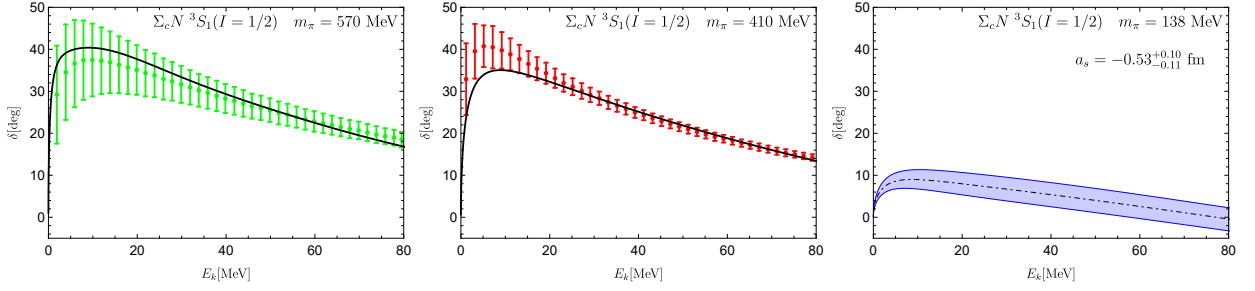


FIG. 6. The chiral extrapolation of phase shift in scenario I with $n = 1$ and $\Lambda = 0.8$ GeV. The green and red points with error bar are the phase shift from lattice QCD [65]. The black solid lines are our fitting results. The third graph is the extrapolated phase shift at the physical pion mass. The blue shadow denotes the uncertainty.

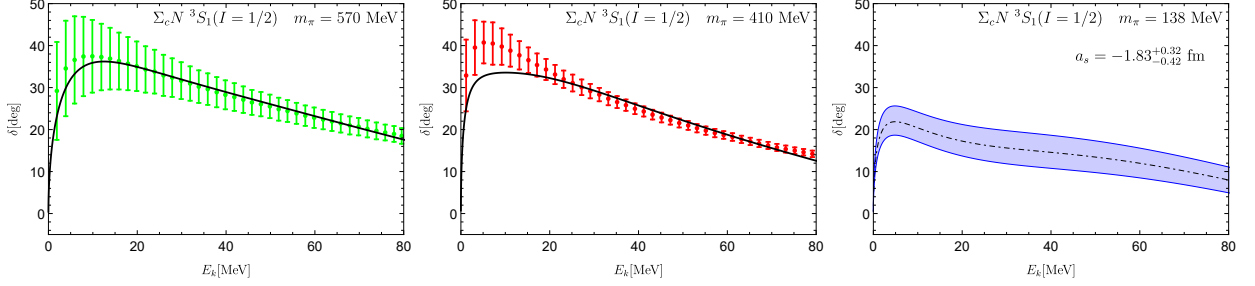


FIG. 7. The chiral extrapolation of phase shift in scenario II with $n = 2$ and $\Lambda = 1.0$ GeV. Notations are the same as those in Fig. 6.

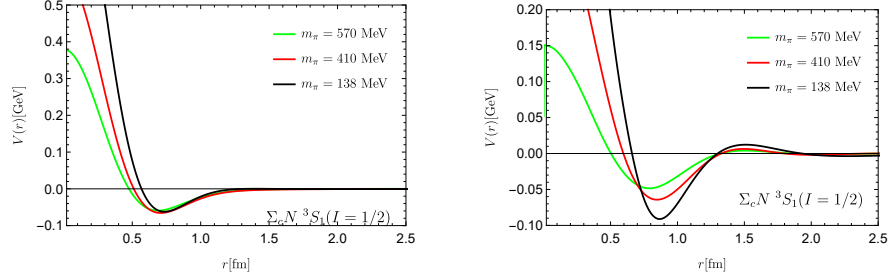


FIG. 8. $\Sigma_c N$ potential in the ${}^3S_1(I = 1/2)$ channel in momentum space. The left one and the right one are the results in scenario I and II, respectively.

the next-to-leading order, we also include the renormalization of vertices, masses and wave functions. In the calculation, the diagrams with Σ_c^* as the intermediate states are taken into consideration. We use our pion mass dependent results to fit the $\Sigma_c N$ [${}^3S_1(I = 1/2)$] phase shifts from HAL QCD with $m_\pi \approx 410$ MeV and $m_\pi \approx 570$ MeV, and then extrapolate the interaction to the physical pion mass.

We choose two different regulators to give the numerical results. In both scenarios, we can fit the phase shifts very well and obtain the similar interaction at the physical pion mass. The potential for $\Sigma_c N$ [${}^3S_1(I = 1/2)$] is weakly attractive in the medium range and repulsive in the short range. The scattering length for this channel is negative, but the attraction is too weak to form a bound state.

Extrapolation of lattice QCD simulation with ChPT works well when the pion mass is as low as 300-400 MeV. When m_π moves very far away from the chiral limit, the higher or-

der terms of the chiral expansion would dominate the truncated expansion making the extrapolation untenable. Fortunately, we adopt some m_π -dependence directly from the lattice simulation like f_π , $g_A M_N$, and M_{Σ_c} , which makes our extrapolation more reliable even for $m_\pi \approx 570$ MeV. There are some approaches which can depict the pion mass dependence beyond the perturbative chiral regime, like the cloudy bag model [80, 81].

In Appendix A, we propose a quark model to estimate the leading order contact interaction for the $\Sigma_c N$ systems. Rather than contracting the specific heavy meson exchange to one point, we assume the local interaction at the quark level. We use SU(3) flavor symmetry to reduce the coupling constants at the quark level and adopt the NN contact interaction as input. We calculate the $\Sigma_c N$ interaction in four S -wave channels with the one-pion-exchange interaction, two-pion exchange interaction and contact interaction estimated

by the quark model. The $^1S_0(I = 3/2)$ channel is the most attractive one and the only one that has the $\Sigma_c N$ bound solution.

In this work, we do not consider the couple-channel effect between $\Sigma_c N$ and $\Lambda_c N$ channels, and the S - D wave mixing due to the tensor force. In the future, investigation on the $Y_c N$ interaction could be promoted by calculating the $\Lambda_c N$ scattering, including the Δ as intermediate states and considering the S - D wave mixing. The framework in this work can be extended to extrapolate the $\Sigma_c^{(*)} \bar{D}^{(*)}$ interaction to investigate the P_c states in the future.

ACKNOWLEDGMENTS

L. Meng is very grateful to G. J. Wang, X. Z. Weng, X. L. Chen and W. Z. Deng for very helpful discussions. This project is supported by the National Natural Science Foundation of China under Grant 11975033.

Appendix A: Using quark model to estimate the contact interaction

In Ref. [65], only the $\Sigma_c N$ interaction with 3S_1 and $I = 1/2$ was calculated. In this section, we use the quark model to estimate the leading order contact terms and give the numerical results for all the S -wave $\Sigma_c N$ interaction.

One purpose to introduce the contact terms is to include the heavy-meson-exchange interaction after integrating out the meson mass. At the quark level, we introduce the contact interaction as,

$$\mathcal{V}_{qq} = c_S(1 + 3\boldsymbol{\tau}_1 \cdot \boldsymbol{\tau}_2) + c_T(1 + 3\boldsymbol{\tau}_1 \cdot \boldsymbol{\tau}_2)\boldsymbol{\sigma}_1 \cdot \boldsymbol{\sigma}_2. \quad (\text{A1})$$

We assume the local interaction is an approximation of the heavy-meson-exchange contribution at quark level when the meson masses are integrated out. The exchanged isospin singlet and isospin triplet belong to the same multiplets in the SU(3) flavor symmetry. Thus, they share the same coupling constants. Since we focus on the interaction of u/d quarks, we can write the exchanged mesons as

$$\mathbb{M} = \boldsymbol{a} \cdot \boldsymbol{\tau} + \frac{1}{\sqrt{3}}f, \quad (\text{A2})$$

where \boldsymbol{a} and f generally represent the isospin triplet and isospin singlet, respectively. Thus, there are only two independent coupling constants in Eq. (A1).

With the quark level interaction, we can calculate the NN and $\Sigma_c N$ contact interaction. We present the relevant matrix elements in Table II. Thus, we could relate the unknown LECs for $\Sigma_c N$ in Eq. (9) to the NN contact interaction with the quark model as a bridge.

For the NN system, the leading order contact interaction reads [12],

$$\mathcal{V}_{NN}^{(0)} = C_S + C_T \boldsymbol{\sigma}_1 \cdot \boldsymbol{\sigma}_2, \quad (\text{A3})$$

where C_S and C_T are the LECs for central potential and spin-spin interaction, respectively. In principle, one also needs to

TABLE II. The matrix elements of the operator $\sum_{i \in h_a, j \in h_b} O_{ij}$, where h_a and h_b are two hadrons. O_{ij} is the two-body interaction operator between quarks.

O_{ij}	1_{ij}	$\boldsymbol{\sigma}_i \cdot \boldsymbol{\sigma}_j$	$\boldsymbol{\tau}_i \cdot \boldsymbol{\tau}_j$	$\boldsymbol{\sigma}_i \cdot \boldsymbol{\sigma}_j \boldsymbol{\tau}_i \cdot \boldsymbol{\tau}_j$
$[NN]_{S=0}^{I=1}$	9	-3	1	$-\frac{25}{3}$
$[NN]_{S=1}^{I=0}$	9	1	-3	$-\frac{25}{3}$
$[\Sigma_c N]_{S=1}^{I=\frac{3}{2}}$	6	$\frac{4}{3}$	2	$\frac{20}{9}$
$[\Sigma_c N]_{S=0}^{I=\frac{3}{2}}$	6	-4	2	$-\frac{20}{3}$
$[\Sigma_c N]_{S=1}^{I=\frac{1}{2}}$	6	$\frac{4}{3}$	-4	$-\frac{40}{9}$
$[\Sigma_c N]_{S=0}^{I=\frac{1}{2}}$	6	-4	-4	$\frac{40}{3}$

construct the isospin-isospin interaction. However, the two nucleons are identical particles and satisfy the Pauli principle. For the S -wave two nucleon system, once the total spin is fixed, the total isospin could be determined consequently. Thus, the isospin-isospin interaction could be absorbed into C_S and C_T . The value of C_S and C_T have been determined by fitting the nucleon scattering phase shift, which is less dependent on the cutoff in the regulator. We take $C_S = -100 \text{ GeV}^{-2}$ and $C_T = 6.5 \text{ GeV}^{-2}$ [12]. The LECs in the leading order $\Sigma_c N$ contact Lagrangians [see Eq. (9)] are then determined as

$$\begin{aligned} C_3 &= -5.21 \text{ GeV}^{-2}, & C_4 &= -5.21 \text{ GeV}^{-2}, \\ \tilde{C}_3 &= 5.19 \text{ GeV}^{-2}, & \tilde{C}_4 &= 25.97 \text{ GeV}^{-2}. \end{aligned} \quad (\text{A4})$$

The $\Sigma_c N$ potentials in coordinate space are presented in Fig. 9. The contribution of the leading order contact term, the one-pion-exchange interaction and the two-pion-exchange contribution are included. With the quark model as a bridge, we could determine the $\Sigma_c N$ effective potentials for all four S -wave channels. The scenarios with different regulators give the similar results.

For the $^3S_1(I = 1/2)$ channel of $\Sigma_c N$, the medium-range interaction is attractive and the short-range interaction is repulsive, which is in accordance with the chiral extrapolation of lattice QCD results. There does not exist the bound solution in this channel. The $^1S_0(I = 1/2)$ channel is strongly repulsive. For the $I = 3/2$ channel, the $\Sigma_c N$ interaction with quantum number 3S_1 is repulsive in the medium range but attractive in the short range. There is no bound solution in this channel. The $^1S_0(I = 3/2)$ channel is the most attractive one. We find a bound solution in this channel,

$$\begin{aligned} E &= -172 \text{ MeV (Scenario I)}, \\ E &= -48 \text{ MeV (Scenario II)}. \end{aligned} \quad (\text{A5})$$

The behaviors of the effective potentials for S -wave $\Sigma_c N$ channels are in accordance with the refined quark model calculation [63]. The approach applied to the contact interaction could also be used to investigate the P_c states [40, 41], in which the $\Lambda_c \bar{D}^{(*)}$ interaction can be related to the $\Sigma_c^{(*)} \bar{D}^{(*)}$ ones.

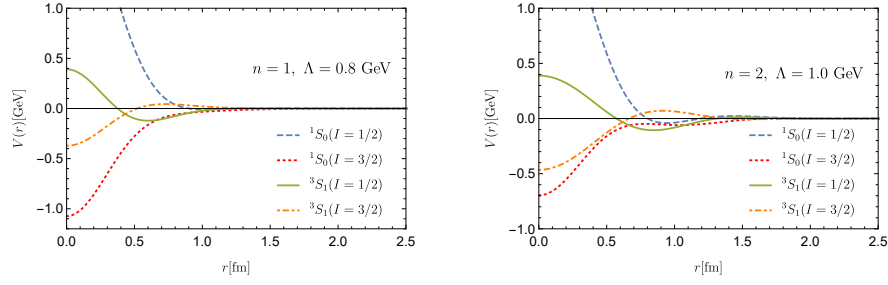


FIG. 9. $\Sigma_c N$ potentials obtained by combining the chiral effective field theory and quark model. The potentials include the leading order contact term estimated in quark model with the NN contact interaction as inputs, the one-pion-exchange interaction and the two-pion-exchange contribution.

Appendix B: Definitions of the loop integrals

We will use the “ $MxBY$ ” to denote the integrals with x light meson propagators and y heavy baryon propagators in the following.

- M1B0

$$i \int \frac{d^d l \lambda^{4-d}}{(2\pi)^d} \frac{\{1, l^\alpha, l^\alpha l^\beta\}}{l^2 - m^2 + i\varepsilon} \equiv \{J_0^c, 0, g^{\alpha\beta} J_{21}^c\} (m), \quad (\text{B1})$$

- M2B0

$$i \int \frac{d^d l \lambda^{4-d}}{(2\pi)^d} \frac{\{1, l^\alpha, l^\alpha l^\beta, l^\alpha l^\beta l^\gamma\}}{(l^2 - m^2 + i\varepsilon) [(l+q)^2 - m^2 + i\varepsilon]} \equiv \{J_0^F, q^\alpha J_{11}^F, q^\alpha q^\beta J_{21}^F + g^{\alpha\beta} J_{22}^F, (g \vee q) J_{31}^F + q^\alpha q^\beta q^\gamma J_{32}^F\} (m, q), \quad (\text{B2})$$

- M1B1

$$i \int \frac{d^d l \lambda^{4-d}}{(2\pi)^d} \frac{\{1, l^\alpha, l^\alpha l^\beta, l^\alpha l^\beta l^\gamma\}}{(v \cdot l + \omega + i\varepsilon) (l^2 - m^2 + i\varepsilon)} \equiv \{J_0^a, v^\alpha J_{11}^a, v^\alpha v^\beta J_{21}^a + g^{\alpha\beta} J_{22}^a, (g \vee v) J_{31}^a + v^\alpha v^\beta v^\gamma J_{32}^a\} (m, \omega), \quad (\text{B3})$$

- M2B1

$$i \int \frac{d^d l \lambda^{4-d}}{(2\pi)^d} \frac{\{1, l^\alpha, l^\alpha l^\beta, l^\alpha l^\beta l^\gamma, l^\alpha l^\beta l^\gamma l^\delta\}}{(v \cdot l + \omega + i\varepsilon) (l^2 - m^2 + i\varepsilon) [(l+q)^2 - m^2 + i\varepsilon]} \equiv \left\{ J_0^T, q^\alpha J_{11}^T + v^\alpha J_{12}^T, g^{\alpha\beta} J_{21}^T + q^\alpha q^\beta J_{22}^T + v^\alpha v^\beta J_{23}^T \right. \\ \left. + (q \vee v) J_{24}^T, (g \vee q) J_{31}^T + q^\alpha q^\beta q^\gamma J_{32}^T + (q^2 \vee v) J_{33}^T + (g \vee v) J_{34}^T + (q \vee v^2) J_{35}^T + v^\alpha v^\beta v^\gamma J_{36}^T, (g \vee g) J_{41}^T \right. \\ \left. + (g \vee q^2) J_{42}^T + q^\alpha q^\beta q^\gamma q^\delta J_{43}^T + (g \vee v^2) J_{44}^T + v^\alpha v^\beta v^\gamma v^\delta J_{45}^T + (q^3 \vee v) J_{46}^T + (q^2 \vee v^2) J_{47}^T + (q \vee v^3) J_{48}^T \right. \\ \left. + (g \vee q \vee v) J_{49}^T \right\} (m, \omega, q), \quad (\text{B4})$$

- M1B2

$$i \int \frac{d^D l \lambda^{4-D}}{(2\pi)^D} \frac{\{1, l^\alpha, l^\alpha l^\beta, l^\alpha l^\beta l^\gamma\}}{(v \cdot l + \omega_1 + i\varepsilon) [(+/-)v \cdot l + \omega_2 + i\varepsilon] (l^2 - m^2 + i\varepsilon)} \\ \equiv \left\{ J_0^{g/h}, v^\alpha J_{11}^{g/h}, v^\alpha v^\beta J_{21}^{g/h} + g^{\alpha\beta} J_{22}^{g/h}, (g \vee v) J_{31}^{g/h} + v^\alpha v^\beta v^\gamma J_{32}^{g/h} \right\} (m, \omega_1, \omega_2), \quad (\text{B5})$$

- M2B2

$$i \int \frac{d^d l \lambda^{4-d}}{(2\pi)^d} \frac{\{1, l^\alpha, l^\alpha l^\beta, l^\alpha l^\beta l^\gamma, l^\alpha l^\beta l^\gamma l^\delta\}}{(v \cdot l + \omega_1 + i\varepsilon) [(+/-)v \cdot l + \omega_2 + i\varepsilon] (l^2 - m^2 + i\varepsilon) [(l+q)^2 - m^2 + i\varepsilon]} \equiv \left\{ J_0^{R/B}, q^\alpha J_{11}^{R/B} + v^\alpha J_{12}^{R/B}, \right.$$

$$\begin{aligned}
& g^{\alpha\beta} J_{21}^{R/B} + q^\alpha q^\beta J_{22}^{R/B} + v^\alpha v^\beta J_{23}^{R/B} + (q \vee v) J_{24}^{R/B}, (g \vee q) J_{31}^{R/B} + q^\alpha q^\beta q^\gamma J_{32}^{R/B} + (q^2 \vee v) J_{33}^{R/B} + (g \vee v) J_{34}^{R/B} \\
& + (q \vee v^2) J_{35}^{R/B} + v^\alpha v^\beta v^\gamma J_{36}^{R/B}, (g \vee g) J_{41}^{R/B} + (g \vee q^2) J_{42}^{R/B} + q^\alpha q^\beta q^\gamma q^\delta J_{43}^{R/B} + (g \vee v^2) J_{44}^{R/B} + v^\alpha v^\beta v^\gamma v^\delta J_{45}^{R/B} \\
& + (q^3 \vee v) J_{46}^{R/B} + (q^2 \vee v^2) J_{47}^{R/B} + (q \vee v^3) J_{48}^{R/B} + (g \vee q \vee v) J_{49}^{R/B} \} (m, \omega_1, \omega_2, q),
\end{aligned} \tag{B6}$$

We use the representation $X \vee Y \vee Z \dots$ to denote the symmetrized tensor structure for simplicity. For example,

$$\begin{aligned}
q \vee v &\equiv q^\alpha v^\beta + q^\beta v^\alpha, \\
g \vee q &\equiv g^{\alpha\beta} q^\gamma + g^{\alpha\gamma} q^\beta + g^{\gamma\beta} q^\alpha, \\
g \vee g &\equiv g^{\alpha\beta} g^{\gamma\delta} + g^{\alpha\gamma} g^{\beta\delta} + g^{\alpha\delta} g^{\beta\gamma}.
\end{aligned} \tag{B7}$$

The final results of these integrals can be found in Refs. [40, 41].

-
- [1] H.-X. Chen, W. Chen, X. Liu, and S.-L. Zhu, *Phys. Rept.* **639**, 1 (2016), arXiv:1601.02092 [hep-ph].
- [2] A. Esposito, A. Pilloni, and A. D. Polosa, *Phys. Rept.* **668**, 1 (2017), arXiv:1611.07920 [hep-ph].
- [3] F.-K. Guo, C. Hanhart, U.-G. Meißner, Q. Wang, Q. Zhao, and B.-S. Zou, *Rev. Mod. Phys.* **90**, 015004 (2018), arXiv:1705.00141 [hep-ph].
- [4] S. L. Olsen, T. Skwarnicki, and D. Zieminska, *Rev. Mod. Phys.* **90**, 015003 (2018), arXiv:1708.04012 [hep-ph].
- [5] Y.-R. Liu, H.-X. Chen, W. Chen, X. Liu, and S.-L. Zhu, *Prog. Part. Nucl. Phys.* **107**, 237 (2019), arXiv:1903.11976 [hep-ph].
- [6] N. Brambilla, S. Eidelman, C. Hanhart, A. Nefediev, C.-P. Shen, C. E. Thomas, A. Vairo, and C.-Z. Yuan, (2019), arXiv:1907.07583 [hep-ex].
- [7] H. Yukawa, *Proc. Phys. Math. Soc. Jap.* **17**, 48 (1935), [Prog. Theor. Phys. Suppl.1,1(1935)].
- [8] R. Machleidt, K. Holinde, and C. Elster, *Phys. Rept.* **149**, 1 (1987).
- [9] V. G. J. Stoks, R. A. M. Klomp, C. P. F. Terheggen, and J. J. de Swart, *Phys. Rev.* **C49**, 2950 (1994), arXiv:nucl-th/9406039 [nucl-th].
- [10] R. B. Wiringa, V. G. J. Stoks, and R. Schiavilla, *Phys. Rev.* **C51**, 38 (1995), arXiv:nucl-th/9408016 [nucl-th].
- [11] E. Epelbaum, H.-W. Hammer, and U.-G. Meißner, *Rev. Mod. Phys.* **81**, 1773 (2009), arXiv:0811.1338 [nucl-th].
- [12] R. Machleidt and D. R. Entem, *Phys. Rept.* **503**, 1 (2011), arXiv:1105.2919 [nucl-th].
- [13] S. Weinberg, *Phys. Lett.* **B251**, 288 (1990).
- [14] S. Weinberg, *Nucl. Phys.* **B363**, 3 (1991).
- [15] M. Oka and K. Yazaki, *Phys. Lett.* **90B**, 41 (1980).
- [16] M. Oka and K. Yazaki, *Prog. Theor. Phys.* **66**, 556 (1981).
- [17] M. Oka and K. Yazaki, *Prog. Theor. Phys.* **66**, 572 (1981).
- [18] A. Faessler, F. Fernandez, G. Lubeck, and K. Shimizu, *Phys. Lett.* **112B**, 201 (1982).
- [19] F. Wang, G.-h. Wu, L.-j. Teng, and J. T. Goldman, *Phys. Rev. Lett.* **69**, 2901 (1992), arXiv:nucl-th/9210002 [nucl-th].
- [20] F. Fernandez, A. Valcarce, U. Straub, and A. Faessler, *J. Phys.* **G19**, 2013 (1993).
- [21] Z.-Y. Zhang, A. Faessler, U. Straub, and L. Ya. Glozman, *Nucl. Phys.* **A578**, 573 (1994).
- [22] D. R. Entem, F. Fernandez, and A. Valcarce, *Phys. Lett.* **B463**, 153 (1999).
- [23] K. Shimizu and L. Ya. Glozman, *Phys. Lett.* **B477**, 59 (2000), arXiv:nucl-th/9906008 [nucl-th].
- [24] K. Nagata and A. Hosaka, *Prog. Theor. Phys.* **111**, 857 (2004), arXiv:hep-ph/0312161 [hep-ph].
- [25] Y. Fujiwara, Y. Suzuki, and C. Nakamoto, *Prog. Part. Nucl. Phys.* **58**, 439 (2007), arXiv:nucl-th/0607013 [nucl-th].
- [26] F. Huang and W. L. Wang, *Phys. Rev.* **D98**, 074018 (2018), arXiv:1810.02120 [nucl-th].
- [27] N. Ishii, S. Aoki, and T. Hatsuda, *Phys. Rev. Lett.* **99**, 022001 (2007), arXiv:nucl-th/0611096 [nucl-th].
- [28] S. Aoki, T. Hatsuda, and N. Ishii, *Prog. Theor. Phys.* **123**, 89 (2010), arXiv:0909.5585 [hep-lat].
- [29] S. Aoki, T. Doi, T. Hatsuda, Y. Ikeda, T. Inoue, N. Ishii, K. Murano, H. Nemura, and K. Sasaki (HAL QCD), *PTEP* **2012**, 01A105 (2012), arXiv:1206.5088 [hep-lat].
- [30] Z.-F. Sun, J. He, X. Liu, Z.-G. Luo, and S.-L. Zhu, *Phys. Rev.* **D84**, 054002 (2011), arXiv:1106.2968 [hep-ph].
- [31] L. Meng, N. Li, and S.-L. Zhu, *Phys. Rev.* **D95**, 114019 (2017), arXiv:1704.01009 [hep-ph].
- [32] L. Meng, N. Li, and S.-L. Zhu, *Eur. Phys. J.* **A54**, 143 (2018), arXiv:1707.03598 [hep-ph].
- [33] B. Yang, L. Meng, and S.-L. Zhu, *Eur. Phys. J.* **A55**, 21 (2019), arXiv:1810.03332 [hep-ph].
- [34] B. Yang, L. Meng, and S.-L. Zhu, (2019), arXiv:1906.04956 [hep-ph].
- [35] R. Chen, Z.-F. Sun, X. Liu, and S.-L. Zhu, *Phys. Rev.* **D100**, 011502 (2019), arXiv:1903.11013 [hep-ph].
- [36] Z.-H. Guo, J. A. Oller, and G. Ros, *Phys. Rev.* **C89**, 014002 (2014), arXiv:1305.5790 [nucl-th].
- [37] Z.-W. Liu, N. Li, and S.-L. Zhu, *Phys. Rev.* **D89**, 074015 (2014), arXiv:1211.3578 [hep-ph].
- [38] H. Xu, B. Wang, Z.-W. Liu, and X. Liu, *Phys. Rev.* **D99**, 014027 (2019), arXiv:1708.06918 [hep-ph].
- [39] B. Wang, Z.-W. Liu, and X. Liu, *Phys. Rev.* **D99**, 036007 (2019), arXiv:1812.04457 [hep-ph].
- [40] L. Meng, B. Wang, G.-J. Wang, and S.-L. Zhu, *Phys. Rev.* **D100**, 014031 (2019), arXiv:1905.04113 [hep-ph].
- [41] B. Wang, L. Meng, and S.-L. Zhu, *JHEP* **11**, 108 (2019), arXiv:1909.13054 [hep-ph].
- [42] X.-L. Ren, K.-W. Li, L.-S. Geng, B.-W. Long, P. Ring, and J. Meng, *Chin. Phys.* **C42**, 014103 (2018), arXiv:1611.08475 [nucl-th].

- [43] J. Song, K.-W. Li, and L.-S. Geng, *Phys. Rev.* **C97**, 065201 (2018), arXiv:1802.04433 [nucl-th].
- [44] J. Haidenbauer, U. G. Meißner, N. Kaiser, and W. Weise, *Eur. Phys. J.* **A53**, 121 (2017), arXiv:1612.03758 [nucl-th].
- [45] J. Haidenbauer and U. G. Meißner, *Eur. Phys. J.* **A55**, 23 (2019), arXiv:1810.04883 [nucl-th].
- [46] J. Haidenbauer, U. G. Meißner, and A. Nogga, (2019), arXiv:1906.11681 [nucl-th].
- [47] A. Hosaka, T. Hyodo, K. Sudoh, Y. Yamaguchi, and S. Yasui, *Prog. Part. Nucl. Phys.* **96**, 88 (2017), arXiv:1606.08685 [hep-ph].
- [48] G. Bhamathi, *Phys. Rev.* **C24**, 1816 (1981).
- [49] H. Bando and S. Nagata, *Prog. Theor. Phys.* **69**, 557 (1983).
- [50] N. I. Starkov and V. A. Tsarev, *HYPERNUCLEAR AND KAON PHYSICS. PROCEEDINGS, INTERNATIONAL SYMPOSIUM, UPTON, USA, SEPTEMBER 9-13, 1985*, *Nucl. Phys.* **A450**, 507C (1986).
- [51] H. Noumi, *Proceedings, 12th International Conference on Hypernuclear and Strange Particle Physics (HYP 2015): Sendai, Japan, September 7-12, 2015*, *JPS Conf. Proc.* **17**, 111003 (2017).
- [52] H. Fujioka *et al.*, (2017), arXiv:1706.07916 [nucl-ex].
- [53] U. Wiedner, *Prog. Part. Nucl. Phys.* **66**, 477 (2011), arXiv:1104.3961 [hep-ex].
- [54] C. H. Cai, L. Li, Y. H. Tan, and P. Z. Ning, *Europhys. Lett.* **64**, 448 (2003).
- [55] K. Tsushima and F. C. Khanna, *J. Phys.* **G30**, 1765 (2004), arXiv:nucl-th/0303073 [nucl-th].
- [56] V. B. Kopeliovich and A. M. Shunderuk, *Proceedings, 9th International Conference on Hypernuclear and strange particle physics (HYP 2006): Mainz, Germany, October 10-14, 2006*, *Eur. Phys. J.* **A33**, 277 (2007), [177(2007)], arXiv:hep-ph/0701249 [HEP-PH].
- [57] H. Garcilazo, A. Valcarce, and T. F. Carams, *Phys. Rev.* **C92**, 024006 (2015), arXiv:1508.03535 [nucl-th].
- [58] I. Vidaa, A. Ramos, and C. E. Jimenez-Tejero, *Phys. Rev.* **C99**, 045208 (2019), arXiv:1901.09644 [nucl-th].
- [59] Y.-R. Liu and M. Oka, *Phys. Rev.* **D85**, 014015 (2012), arXiv:1103.4624 [hep-ph].
- [60] S. Maeda, M. Oka, A. Yokota, E. Hiyama, and Y.-R. Liu, *PTEP* **2016**, 023D02 (2016), arXiv:1509.02445 [nucl-th].
- [61] S. Maeda, M. Oka, and Y.-R. Liu, *Phys. Rev.* **C98**, 035203 (2018), arXiv:1803.11349 [nucl-th].
- [62] H. Huang, J. Ping, and F. Wang, *Phys. Rev.* **C87**, 034002 (2013).
- [63] H. Garcilazo, A. Valcarce, and T. F. Carams, *Eur. Phys. J.* **C79**, 598 (2019), arXiv:1907.05022 [hep-ph].
- [64] T. Miyamoto *et al.*, *Nucl. Phys.* **A971**, 113 (2018), arXiv:1710.05545 [hep-lat].
- [65] T. Miyamoto (HAL QCD), *Proceedings, 17th International Conference on Hadron Spectroscopy and Structure (Hadron 2017): Salamanca, Spain, September 25-29, 2017*, *PoS Hadron2017*, 146 (2018).
- [66] J. Haidenbauer and G. Krein, *Eur. Phys. J.* **A54**, 199 (2018), arXiv:1711.06470 [hep-ph].
- [67] G. Krein, A. W. Thomas, and K. Tsushima, *Prog. Part. Nucl. Phys.* **100**, 161 (2018), arXiv:1706.02688 [hep-ph].
- [68] N. Kaiser, R. Brockmann, and W. Weise, *Nucl. Phys.* **A625**, 758 (1997), arXiv:nucl-th/9706045 [nucl-th].
- [69] H. Krebs, E. Epelbaum, and U.-G. Meissner, *Eur. Phys. J.* **A32**, 127 (2007), arXiv:nucl-th/0703087 [nucl-th].
- [70] E. Epelbaum, W. Glockle, and U.-G. Meissner, *Nucl. Phys.* **A747**, 362 (2005), arXiv:nucl-th/0405048 [nucl-th].
- [71] S. Drr *et al.* (Budapest-Marseille-Wuppertal), *Phys. Rev.* **D90**, 114504 (2014), arXiv:1310.3626 [hep-lat].
- [72] M. Procura, B. U. Musch, T. R. Hemmert, and W. Weise, *Phys. Rev.* **D75**, 014503 (2007), arXiv:hep-lat/0610105 [hep-lat].
- [73] W. Detmold, C. J. D. Lin, and S. Meinel, *Phys. Rev.* **D85**, 114508 (2012), arXiv:1203.3378 [hep-lat].
- [74] C. Alexandrou, K. Hadjiyiannakou, and C. Kallidonis, *Phys. Rev.* **D94**, 034502 (2016), arXiv:1606.01650 [hep-lat].
- [75] T. R. Hemmert, B. R. Holstein, and J. Kambor, *J. Phys.* **G24**, 1831 (1998), arXiv:hep-ph/9712496 [hep-ph].
- [76] D. B. Leinweber, A. W. Thomas, K. Tsushima, and S. V. Wright, *Phys. Rev.* **D64**, 094502 (2001), arXiv:hep-lat/0104013 [hep-lat].
- [77] M. Werner *et al.*, (2019), arXiv:1907.01237 [hep-lat].
- [78] C. Ordonez, L. Ray, and U. van Kolck, *Phys. Rev.* **C53**, 2086 (1996), arXiv:hep-ph/9511380 [hep-ph].
- [79] M. S. Stern, *Comput. Phys. Commun.* **17**, 365 (1979).
- [80] D. B. Leinweber, D.-H. Lu, and A. W. Thomas, *Phys. Rev.* **D60**, 034014 (1999), arXiv:hep-lat/9810005 [hep-lat].
- [81] D. B. Leinweber, A. W. Thomas, K. Tsushima, and S. V. Wright, *Phys. Rev.* **D61**, 074502 (2000), arXiv:hep-lat/9906027 [hep-lat].